Materials Advances

ROYAL SOCIETY OF CHEMISTRY

PAPER

View Article Online
View Journal

Cite this: DOI: 10.1039/d5ma01052g

Highly stable chiral bimetallic mesoporous platinum–ruthenium electrodes for enantioselective recognition

Sopon Butcha, *[a] Natthaphong Kaewwan,[b] Krissanapat Yomthong,[b] Zikkawas Pasom,[bc] Alexander Kuhn [bc] and Chularat Wattanakit [b]

Received 13th September 2025,
Accepted 22nd February 2026

DOI: 10.1039/d5ma01052g

rsc.li/materials-advances

Chiral bimetallic mesoporous platinum–ruthenium (Pt–Ru) alloy films have been successfully synthesised *via* co-electrodeposition. When used as electrodes, these alloys show enhanced electrochemical activity, combined with an exceptional electrochemical stability, particularly under harsh oxidative conditions. The electrodes efficiently discriminate between mandelic acid enantiomers, with an enantioselectivity ratio of over 6, nearly triple that of previously reported chiral encoded platinum surfaces. Even after severe oxidative treatment under conditions that typically degrade the chiral properties, the Pt–Ru electrodes retain their chiral features. This unprecedented stability opens up interesting avenues for using these alloys as robust and reliable tools for real-world applications related to chiral technologies.

Introduction

Chirality is vital in numerous scientific fields, especially in chemistry, biology, and materials science. Chiral molecules, which exhibit non-superimposable mirror image properties, typically show distinct biological effects. One enantiomer can be useful, whereas the opposite stereoisomer might be even toxic. Accordingly, it is important to accurately synthesize or recognize them as enantiomerically pure compounds (EPCs).[1,2] One possibility to carry out this task is to use electrochemical approaches. In this context, mesoporous metals are an interesting choice as electrode materials, due to their large active surface area,[3] which can considerably improve the performance in terms of mass transport limitations, and host an increased number of recognition sites.[4] Therefore, mesoporous metals have been proposed for designing sensors[5] and catalytically active surfaces for chiral synthesis.[6] However, using classic mesoporous metals for these applications presents several challenges, for example, related to surface poisoning with by-products of the involved redox reactions, such as carbon dioxide or carbon monoxide,[7,8] and deficient electrochemical stability of metals. To overcome these limitations, new types of mesoporous metals should be studied to adapt them to practical applications.

Earlier studies found that various types of mesoporous metals can be endowed with chiral features, including platinum (Pt),[5,6] nickel (Ni),[9] and platinum–iridium (Pt–Ir) alloys.[10] These materials have been successfully prepared by electrodeposition from a plating gel containing self-assembled non-ionic surfactants as mesoporogens, metal precursors,[3] and chiral target molecules that can generate specific chiral recognition sites in the metal structure.[5] This results in a metal matrix with a high active surface area, low-symmetry, and a certain chiral character.[11] With these materials, significant chiral discrimination can be achieved when using them for enantioselective electroanalysis and electrosynthesis.[10,12]

The previously reported chiral imprinted mesoporous metals have been mostly used for electroreduction processes,[10] while electrooxidation reactions for generating chiral compounds have not been explored so far. This is due, at least partly, to the fact that in an oxidative regime, the imprinted chiral information might be erased by a rearrangement of the metal atoms,[10] leading to very modest long-term electrochemical stability – a critical barrier to sustained performance.

One way to circumvent these problems is to use alloys instead of single metal structures, as they often show better stability. For example, bimetallic platinum–ruthenium (Pt–Ru) has demonstrated significant electrochemical stability even under oxidizing conditions, thus being a popular electrocatalyst, especially for electrooxidation.[13,14] It has been shown that a mesoporous version can be generated by the electrodeposition of Pt and Ru salts dissolved in a solution containing a non-ionic surfactant.[15,16]

Accordingly, in this contribution, chiral bimetallic mesoporous Pt–Ru surfaces were generated by co-electrodeposition

[a] *Department of Chemistry, Faculty of Science and Technology, Thammasat University, 12120, Pathum Thani, Thailand. E-mail: soponb22@tu.ac.th*
[b] *School of Energy Science and Engineering, Vidyasirimedhi Institute of Science and Technology, 21210, Rayong, Thailand*
[c] *University of Bordeaux, CNRS, Bordeaux INP, ISM UMR 5255, 33607, Pessac, France*

of Pt and Ru salts in the simultaneous presence of a non-ionic surfactant and chiral templates. The results reveal that the prepared chiral Pt–Ru allows for the electrochemical discrimination of the corresponding enantiomers with a significantly improved stability.

Results and discussion

Synthesis and characterization of chiral-imprinted bimetallic mesoporous Pt–Ru electrodes

Scheme 1 illustrates the preparation steps of chiral bimetallic mesoporous Pt–Ru electrodes. At first, the alloy was successfully synthesized by co-electrodeposition from a mixture of Pt and Ru salts, [$PtCl_6^{2-}$] and [$RuCl_3$], with an initial atomic ratio of 40Pt : 60Ru, in the presence of a lyotropic liquid crystal phase (LLC). The non-ionic surfactant, Brij® 58, is organized in a self-assembled hexagonal structure (H_1), and the chiral template is preferentially adsorbed at the outer surface of the surfactant columns.[5,15,16] Electrodeposition leads to the formation of bimetallic Pt–Ru structures around the assembled templates, forming mesoporous channels and enantioselective recognition sites after template removal. In the present work, mandelic acid (MA) was employed as the chiral template, and it can be completely removed from the Pt–Ru electrodes after the electrodeposition step, as evidenced by UV-vis spectra recorded with the different washing solutions as described already in previous reports. After overnight washing (the same washing protocol for the current chiral Pt–Ru alloy), no characteristic absorption bands of MA were observed, confirming the removal of the template upon extended washing.[17]

For the co-electrodeposition, different reduction potentials were tested, ranging from −0.20 to −0.15 and −0.10 V (*vs.* Ag/AgCl), and the thickness of the final Pt–Ru was controlled by employing different charge densities from 1 to 8 C cm^{-2}. In brief, to obtain a well-controlled homogeneous deposition of metal films, the deposition of mesoporous Pt–Ru electrodes at −0.10 V and an injected charge density of 4 C cm^{-2} was chosen, as separately discussed in the SI, Fig. S1–S4.[5,18] The field emission scanning electron microscopy (FE-SEM) image shows a smooth external surface of the deposited Pt–Ru layers with a thickness of approximately 500 nm (Fig. 1(a)).

The ratio between Pt and Ru is also a crucial parameter for achieving high electrooxidation activity. As shown in Fig. S5, a range of Pt–Ru compositions was initially explored during the synthesis step, namely 80Pt:20Ru, 60Pt:40Ru, 40Pt:60Ru, and 20Pt:80Ru. Following the electrodeposition from plating gels with these atomic ratios, the gel with 60Pt:40Ru resulted in the highest current density for MA electrooxidation among all the samples investigated. An actual composition of the final deposit, recorded with an energy-dispersive X-ray spectrometer (FE-SEM/EDS), reveals an elemental composition of Pt:Ru with an at% ratio of approximately 50 : 50 (Table S1). Importantly,

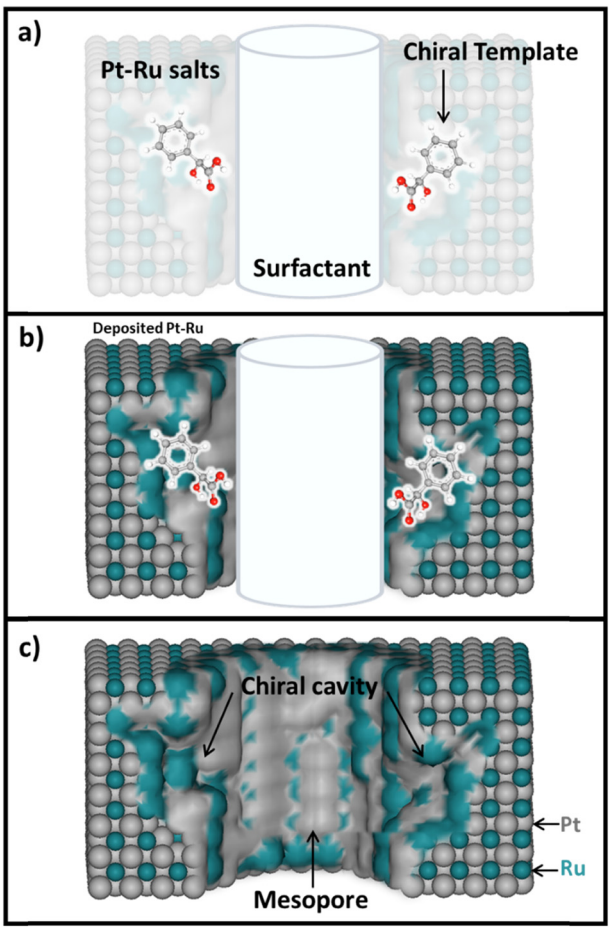

Scheme 1 Synthesis of chiral bimetallic mesoporous Pt–Ru electrodes: (a) electroplating gel containing Pt and Ru salts, a self-assembled hexagonal structure of non-ionic surfactants, and chiral templates; (b) and (c) the chiral bimetallic mesoporous Pt–Ru structures grown around the assembled templates after co-electrodeposition and template removal, respectively.

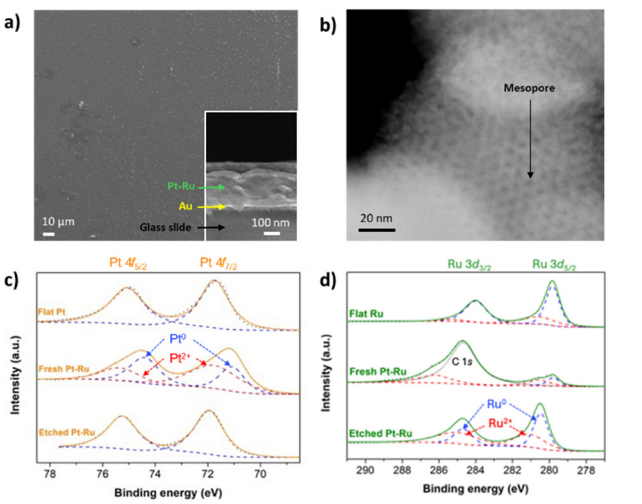

Fig. 1 Characterization of chiral bimetallic mesoporous Pt–Ru electrodes: (a) top-view and cross-sectional (inset) FE-SEM images of the Pt–Ru film (deposition charge density: 4 C cm^{-2}); (b) HADDF-STEM image of an ultra-thin Pt–Ru film; and (c) and (d) narrow-scan XPS spectra of the fresh and etched Pt–Ru electrode compared with monometallic Pt and Ru in the binding energy (eV) region of Pt 4f and Ru 3d, respectively.

this Ru content showed the highest electrooxidation activity, and since Ru itself has a better electrochemical stability than Pt, the overall performance of such a bimetallic layer can be enhanced.[19] Therefore, this Pt/Ru ratio has been chosen as an optimal value for our studies.

The Pt–Ru films reveal a well-ordered hexagonal mesoporous structure with a diameter of 4.7 ± 0.2 nm, as illustrated by the high-angle annular dark-field scanning transmission electron microscopy (HADDF-STEM) image (Fig. 1(b)). X-ray diffraction (XRD) analysis was employed to examine the crystalline structure of the samples. Fig. S6(a) illustrates the XRD patterns of the resulting Pt–Ru, compared with the signals of individual Ru and Pt. For monometallic Pt, the two diffraction peaks at approximate 2θ values of 40.1° and 46.5° align with conventional diffraction patterns for standard platinum (JCPDS 65-2868), exhibiting a face-centred cubic (fcc) structure in the (111) and (200) planes, respectively.[20] Three diffraction peaks are observed at approximate 2θ values of 38.4°, 44.0°, and 58.3°, which is consistent with the conventional diffraction patterns of the standard Ru (JCPDS 65-1863), corresponding to a hexagonal close-packed (hcp) structure in the (100), (101), and (102) planes, respectively.[21] Notably, Pt–Ru samples exhibit two diffraction peaks of Ru(100) and (101) planes that are comparable to that of the Ru crystal structure, suggesting that Pt atoms are uniformly integrated into the Ru hcp lattice. Compared to the typical diffraction pattern of pure Ru, the diffraction peaks of Pt–Ru exhibit a minor shift to higher angles, particularly from 44.0° to 44.3°, indicating an alloyed structure.[22] Additionally, peaks of ruthenium oxides (RuO_2) are detectable at 2θ of 36.0° (101) and 52.0° (211), indicating the generation of mixed phases between the Pt–Ru alloy and RuO_2.[23]

Furthermore, the *d*-spacing values are determined following Bragg's law ($2d \sin\theta = n\lambda$), as presented in Table S2 to confirm the unit cell expansion in the bimetallic alloys. The results indicate that the bimetallic Pt–Ru exhibits a value of 0.235 nm at 38.3°, identical to Ru (100), and 0.204 nm at 44.3°, which is notably lower than the value of 0.210 nm obtained for isolated Ru(101). These results also correlate with the values measured with high-resolution transmission electron microscopy (HR-TEM) of the ultra-thin Pt–Ru film (Fig. S6(b)). The Pt(111) crystalline plane exhibits a *d*-spacing value of 0.220 nm. The *d*-spacing value of 0.201 nm aligns with the XRD results obtained with deposited Pt–Ru at 44.3°. These observations confirm the successful formation of alloyed Pt–Ru structures.

In addition, X-ray photoelectron spectroscopy (XPS) reveals bimetallic Pt–Ru states and surface compositions. Wide-scan XPS spectra (Fig. S7(a)) show characteristic signals of both Ru and O, implying the presence of RuO_2 on fresh Pt–Ru surfaces. However, after etching the Pt–Ru surfaces for 5 s, Pt becomes increasingly visible, indicating mixed Pt and Ru phases, and the O content significantly decreases, implying that the oxide layer disappears. Similarly, fresh Pt–Ru exhibits the doublet characteristics of Pt^0 at 71.0 and 74.3 eV, which correspond to monometallic Pt having doublet bands at 71.8 eV (Pt $4f_{7/2}$) and 75.1 eV (Pt $4f_{5/2}$) (Fig. 1(c)), and Pt^{2+} having doublet bands at 71.9 and 75.4 eV, which is characteristic of PtO_x.[24,25] Also, fresh Pt–Ru has a doublet band at around 279.9 eV (Ru $3d_{5/2}$) and 284.0 eV (Ru $3d_{3/2}$) (Fig. 1(d)),[26,27] but it shows a prominent content of Ru^{2+} species (280.6 and 286.0 eV), which confirms the presence of RuO_2 species on the electrode surface. The results correlate with the XRD pattern, wide-scan XPS data, and the Ru–O phase in the O 1s region (Fig. S7(b)).[28] However, the etched Pt–Ru shows predominant Pt^0 characteristics and highly pure Ru^0 phases. Moreover, after etching deeper into the electrode layer, the doublet band positions of both Pt 4f and Ru 3d are significantly shifted to higher BE, indicating the formation of a Pt–Ru alloy due to the altered electronic structure of Pt and Ru atoms.[25,29] In addition, elemental analysis of etched Pt–Ru samples using XPS reveals a surface species atomic ratio of 25Pt : 75Ru, which is significantly different from the atomic ratio of 50Pt : 50Ru of the bulk Pt–Ru structures detected by FE-SEM/EDS, due to the gradient alloyed Pt–Ru structures. The observed reduction in the Pt content is due to the fact that XPS detects the outermost surface layer, while the Pt–Ru alloy tends to form deeper within the bimetallic Pt–Ru film. This phenomenon is attributed to the rapid electroreduction of Pt salt at the beginning of the deposition process, which leads to its gradual depletion near the growing interface. Thus, the initial stages of deposition yield a film with a higher concentration of Pt, but as the process continues, the amount of Pt incorporated into the film decreases progressively.

Electrochemical stability test of chiral imprinted Pt–Ru surfaces

The electrochemical stability of the chiral imprinted Pt–Ru electrodes was studied with the help of a chiral redox probe.[9,10] For generating chiral mesoporous Pt–Ru, the alloy was imprinted with either (*R*)- or (*S*)-mandelic acid (MA). Prior to analysis, the solution was purged with nitrogen gas for 30 min, and the electrode was activated at −0.1 V for 30 s.[12] The electrochemical recognition of MA was performed with differential pulse voltammetry (DPV), using 10 mM of (*S*)-MA (red line) or (*R*)-MA (black line) dissolved in 10 mM HCl as a supporting electrolyte at a pH of 1.4.[10,17]

Initially, there is a significant difference in current densities when comparing the MA solution and the pure HCl supporting solution (dashed line, blank) for a non-imprinted (N-imp) mesoporous Pt–Ru alloy (Fig. S8), suggesting that Cl^- anion adsorption on the electrode does not substantially affect the interaction of the chiral molecules with the metal surface.[5,10] A broad peak related to MA oxidation is observed between 0.45 and 0.55 V[17] (Scheme S1). As expected, N-imp mesoporous Pt–Ru does not distinguish (*R*)-MA from (*S*)-MA (Fig. S8). In contrast, a (*S*)-MA imprinted (*S*-imp) Pt–Ru film exhibits a much higher current density when (*S*)-MA is present in solution compared to the experiment with its antipode (Fig. 2(a)). Conversely, the (*R*)-MA imprinted (*R*-imp) Pt–Ru alloy reacts preferentially with the (*R*)-MA enantiomer, as demonstrated by the higher anodic peak compared to that of (*S*)-MA (Fig. 2(c)).

Subsequently, both *S*-imp and *R*-imp Pt–Ru alloys were further examined for electrochemical stability by eliminating on purpose the chiral information present in the metal matrix

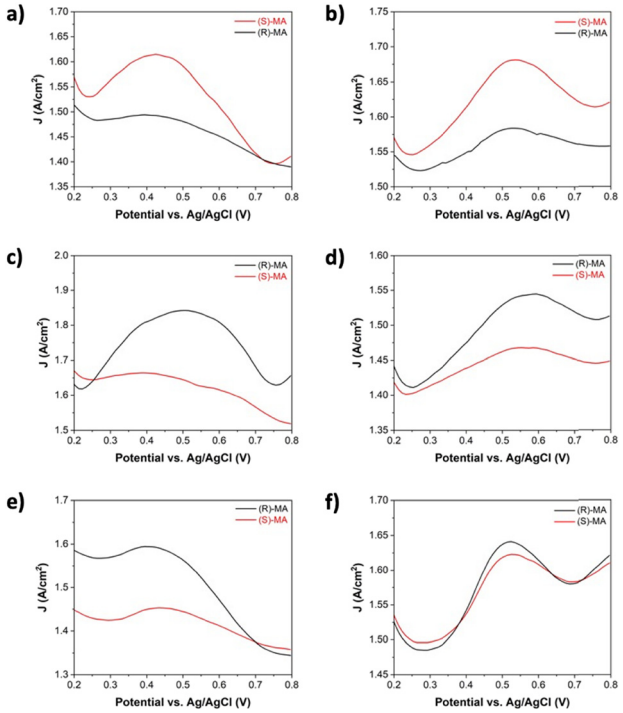

Fig. 2 Differential pulse voltammograms (DPVs) of the electrooxidation of MA on different chiral encoded metal electrodes: (a) fresh (*S*)-MA imprinted (*S*-imp) Pt–Ru; (b) erased *S*-imp Pt–Ru electrodes for 10 cycles; (c) fresh (*R*)-MA imprinted (*R*-imp) Pt–Ru; (d) erased *R*-imp Pt–Ru electrodes for 10 cycles; (e) fresh (*R*)-MA imprinted Pt; and (f) erased (*R*)-MA imprinted Pt for 10 cycles. The DPV was run in 10 mM (*R*)-MA (black) and (*S*)-MA (red) dissolved in 10 mM HCl supporting electrolyte, and chiral information was erased by the CV scan in 0.5 M H_2SO_4 solution at a scan rate of 100 mV s^{-1} from −0.25 to +1.40 V for 10 cycles.

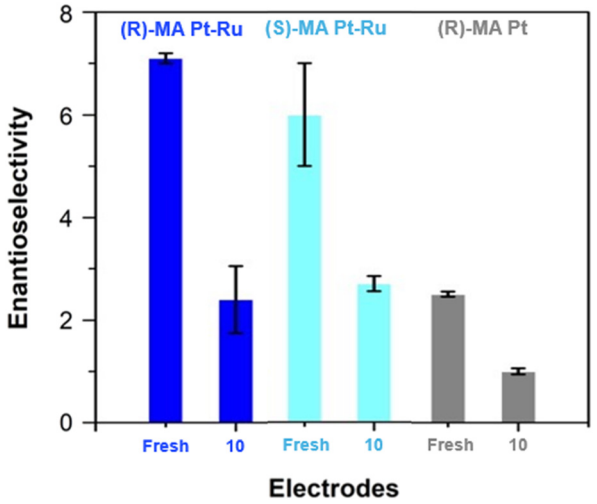

Fig. 3 Enantioselectivity ratios from the various chiral recognition experiments, including (*R*)-MA and (*S*)-MA imprinted Pt–Ru and (*R*)-MA imprinted Pt, for freshly prepared electrodes and after ten potential cycles to erase the chiral features by oxidation.

by applying harsh oxidizing conditions during sequential CV scans in the potential range from −0.25 V to +1.40 V in 0.5 M H_2SO_4.[10] Interestingly, even after 10 CV cycles, both Pt–Ru electrodes can retain their chiral discrimination features, as shown by a significantly higher anodic peak for the imprinted enantiomer (Fig. 2(b) and (d)).

In order to confirm the superior performance of the alloy, its chiral recognition features have been compared with those of imprinted monometallic Pt. Although the *R*-imp Pt electrode can discriminate MA enantiomers as illustrated in Fig. 2(e), the chiral information completely disappears after only 10 potential cycles, evidenced by almost identical DPV signals recorded in the (*S*)-MA and (*R*)-MA solutions (Fig. 2(f)). In fact, monometallic Pt generally starts to get oxidized at potential values exceeding +0.65 V,[5] accompanied by a reorganisation of the surface atoms, leading to the degradation of the chiral information already after the very first cycles.[10] These findings demonstrate a substantial increase in electrochemical stability, which might be due to an alternation of the electronic structure of the bimetallic Pt–Ru alloy in comparison to the pure Pt metal, evidenced by the XRD and XPS results.

Furthermore, even after attempting to destroy the chiral information for the additional 10 cycles (a total of 20 cycles, Fig. S9(a) and S10(a)), Pt–Ru can retain its chiral features, emphasizing the stability of this alloy. The electrodes were further oxidized for up to 30 CV cycles. Fig. S9(b) and S10(b) show the almost identical electrooxidation signals of the two enantiomers, implying that imprinted Pt–Ru electrodes lose all chiral information under these harsh oxidative conditions. To sum up, all these findings suggest that bimetallic mesoporous Pt–Ru electrodes are electrochemically stable against harsh oxidizing conditions.

The superior electrochemical stability of the chiral Pt–Ru alloys, compared with the chiral monometallic Pt, can be further illustrated by the degree of chiral recognition ability, which is quantified by analysing the integrated peak areas of the DPV signals related to MA electrooxidation, as summarized in Fig. 3 and Table S3.[12] The relative peak areas between the two MA enantiomers, either (*R*)-MA/(*S*)-MA or (*S*)-MA/(*R*)-MA, have been evaluated. The values for fresh bimetallic Pt–Ru electrodes encoded with (*R*)-MA and (*S*)-MA are approximately 7.1 ± 0.1 and 6.0 ± 1.0, respectively. After partially erasing the chiral information by potential scanning for 10 cycles, there is a significant decrease in the degree of chiral recognition ability, reaching approximately 2.6 in both cases. However, and most importantly, imprinted monometallic Pt, which initially already has a much lower recognition ability, loses its chiral features completely after an identical oxidizing treatment. This confirms the superior electrochemical performance of bimetallic Pt–Ru, even when the electrodes are exposed to drastic oxidizing conditions.

Conclusion

In conclusion, chiral-encoded bimetallic mesoporous Pt–Ru layers were successfully synthesized by co-electroreduction of Pt and Ru salts in the simultaneous presence of a lyotropic liquid crystal and mandelic acid enantiomers as chiral model

templates. The bimetallic Pt–Ru forms an alloy phase of Pt and Ru with a well-ordered hexagonal porous structure. When mandelic acid is encoded, the chiral information is preserved even after the template removal. The chiral bimetallic Pt–Ru films exhibit strong enantioselective recognition properties with a remarkably higher electrochemical stability compared to monometallic Pt. These results illustrate the advantages of using bimetallic materials instead of the pure metal analogues, allowing for overcoming some of the current challenges when using advanced materials in chiral technologies for which long-term stability of the encoded chiral information is mandatory. Especially for the Pt–Ru alloy system, investigated in the present study, we anticipate that the use of such films can be extended also to other more complex and pharmaceutically relevant compounds, as we have already demonstrated in previous studies for analogous, but less stable metal layers.[30]

Author contributions

S. B. performed data collection, writing of the original draft, and funding acquisition. N. K. and K. Y. performed experiments and data collection. Z. P. performed material characterization. A. K. contributed to supervision, and writing and editing of the manuscript. C. W. contributed to supervision, funding acquisition, and writing and editing of the manuscript.

Conflicts of interest

There are no conflicts to declare.

Data availability

The data supporting this article have been included as part of the supplementary information (SI). Supplementary information is available. See DOI: https://doi.org/10.1039/d5ma01052g.

Acknowledgements

The authors gratefully acknowledge the financial support provided by the National Research Council of Thailand (NRCT) (contract number: N42A660983), the Franco-Thai Young Talent Research Fellowship Program (contract number: B13F670125), the Faculty of Science and Technology, Thammasat University (contract number: SciGR 29/2568), the Program Management Unit for Human Resources & Institutional Development, Research, and Innovation (grant number: B41G680026, Global League), the Air Force Office of Scientific Research Unit (Award R&D Grant No. FA2386-23-1-4015) and the CNRS through the IRP project ChiraChem, as well as the French Academy of Science. We also acknowledge the Frontier Research Center (FRC) at Vidyasirimedhi Institute of Science and Technology (VISTEC) for providing all characterization equipment.

References

1 R. Naaman, Y. Paltiel and D. H. Waldeck, Chiral molecules and the spin selectivity effect, *J. Phys. Chem. Lett.*, 2020, **11**, 3660–3666.
2 M. Arabi, A. Ostovan, Y. Wang, R. Mei, L. Fu, J. Li, X. Wang and L. Chen, Chiral molecular imprinting-based SERS detection strategy for absolute enantiomeric discrimination, *Nat. Commun.*, 2022, **13**, 5757.
3 G. S. Attard, P. N. Bartlett, N. R. Coleman, J. M. Elliott, J. R. Owen and J. H. Wang, Mesoporous platinum films from lyotropic liquid crystalline phases, *Science*, 1997, **278**, 838–840.
4 C. Wattanakit and A. Kuhn, Encoding chiral molecular information in metal structures, *Chem. – Eur. J.*, 2020, **26**, 2993–3003.
5 C. Wattanakit, Y. B. S. Côme, V. Lapeyre, P. A. Bopp, M. Heim, S. Yadnum, S. Nokbin, C. Warakulwit, J. Limtrakul and A. Kuhn, Enantioselective recognition at mesoporous chiral metal surfaces, *Nat. Commun.*, 2014, **5**, 3325.
6 S. Butcha, V. Lapeyre, C. Wattanakit and A. Kuhn, Self-assembled monolayer protection of chiral-imprinted mesoporous platinum electrodes for highly enantioselective synthesis, *Chem. Sci.*, 2022, **13**, 2339–2346.
7 M. Borazjani, A. Mehdinia and A. Jabbari, An enantioselective electrochemical sensor for simultaneous determination of mandelic acid enantiomers using dexamethasone-based chiral nanocomposite coupled with chemometrics method, *J. Electroanal. Chem.*, 2017, **805**, 83–90.
8 K. Matsuoka, Y. Iriyama, T. Abe, M. Matsuoka and Z. Ogumi, Electro-oxidation of methanol and ethylene glycol on platinum in alkaline solution: poisoning effects and product analysis, *Electrochim. Acta*, 2005, **51**, 1085–1090.
9 S. Assavapanumat, M. Ketkaew, A. Kuhn and C. Wattanakit, Synthesis, characterization, and electrochemical applications of chiral imprinted mesoporous Ni surfaces, *J. Am. Chem. Soc.*, 2019, **141**, 18870–18876.
10 S. Butcha, S. Assavapanumat, S. Ittisanronnachai, V. Lapeyre, C. Wattanakit and A. Kuhn, Nanoengineered chiral Pt-Ir alloys for high-performance enantioselective electrosynthesis, *Nat. Commun.*, 2021, **12**, 1314.
11 N. Shukla and A. J. Gellman, Chiral metal surfaces for enantioselective processes, *Nat. Mater.*, 2020, **19**, 939–945.
12 S. Butcha, J. Yu, Z. Pasom, B. Goudeau, C. Wattanakit, N. Sojic and A. Kuhn, Electrochemiluminescent enantioselective detection with chiral-imprinted mesoporous metal surfaces, *Chem. Commun.*, 2022, **58**, 10707–10710.
13 C. Long, K. Wang, Y. Shi, Z. Yang, X. Zhang, Y. Zhang, J. Han, Y. Bao, L. Chang, S. Liu and Z. Tang, Tuning the electronic structure of PtRu bimetallic nanoparticles for promoting the hydrogen oxidation reaction in alkaline media, *Inorg. Chem. Front.*, 2019, **6**, 2900–2905.
14 G. Vishwakshan Reddy, P. Raghavendra, B. Ankamwar, P. Sri Chandana, S. M. Senthil Kumar and L. Subramanyam Sarma, Ultrafine Pt–Ru bimetallic nanoparticles anchored

on reduced graphene oxide sheets as highly active electrocatalysts for methanol oxidation, *Mater. Chem. Front.*, 2017, **1**, 757–766.

15 J. Jiang and A. Kucernak, Mesoporous microspheres composed of PtRu alloy, *Chem. Mater.*, 2004, **16**, 1362–1367.

16 H. Wang, M. Imura, Y. Nemoto, L. Wang, H. Y. Jeong, T. Yokoshima, O. Terasaki and Y. Yamauchi, Electrochemical design of mesoporous Pt–Ru alloy films with various compositions toward superior electrocatalytic performance, *Chem. – Eur. J.*, 2012, **18**, 13142–13148.

17 T. Yutthalekha, C. Wattanakit, V. Lapeyre, S. Nokbin, C. Warakulwit, J. Limtrakul and A. Kuhn, Asymmetric synthesis using chiral-encoded metal, *Nat. Commun.*, 2016, **7**(1), 12678.

18 X. Chen, H. Wang, Y. Wang, Q. Bai, Y. Gao and Z. Zhang, Synthesis and electrocatalytic performance of multicomponent nanoporous PtRuCuW alloy for direct methanol fuel cells, *Catalysts*, 2015, **5**, 1003–1015.

19 D. Chu and S. Gilman, Methanol electro-oxidation on unsupported Pt-Ru alloys at different temperatures, *J. Electrochem. Soc.*, 1996, **143**, 1685.

20 X. Zhang, B. Yan, L. Peng, J. Zhao and J. Zheng, Controllable synthesis of Pt nanoparticles on graphene oxide nanosheets and its application for electrochemical determination of dopamine, *ChemistrySelect*, 2023, **8**, e202204022.

21 X. Liu, G. Jiang, Y. Tan, S. Luo, M. Xu, Y. Jia, P. Lu and Y. He, Highly-dispersed ruthenium precursors via a self-assembly-assisted synthesis of uniform ruthenium nanoparticles for superior hydrogen evolution reaction, *RSC Adv.*, 2020, **10**, 14313–14316.

22 Q. Zhou and C. Xu, Nanoporous PtRu alloys with unique catalytic activity toward hydrolytic dehydrogenation of ammonia borane, *Chem. – Asian J.*, 2016, **11**, 705–712.

23 T. D. Nguyen, G. G. Scherer and Z. J. Xu, A facile synthesis of size-controllable IrO_2 and RuO_2 nanoparticles for the oxygen evolution reaction, *Electrocatalysis*, 2016, **7**(5), 420–427.

24 N. Jiang, B. Huang, M. Wang, Y. Chen, Q. Yu and L. Guan, Universal and energy-efficient approach to synthesize Pt-rare earth metal alloys for proton exchange membrane fuel cell, *Adv. Sci.*, 2024, **11**, 2305110.

25 Y. Cong, F. Meng, X. Wang, H. Wang, D. Dou, C. Li and Q. Zhao, Uniform $PtRu_{0.6}$ nanoparticles supported on nitrogen-doped carbon obtained from ZIF-8/GO hybrid with remarkable alkaline hydrogen oxidation activity, *J. Electron. Mater.*, 2023, **52**, 2388–2395.

26 M. Damayanti, T. Sritharan, Z. H. Gan, S. G. Mhaisalkar, N. Jiang and L. Chan, Ruthenium barrier/seed layer for Cu/low-κ metallization: crystallographic texture, roughness, diffusion, and adhesion, *J. Electrochem. Soc.*, 2006, **153**, J41.

27 E. A. Paoli, F. Masini, R. Frydendal, D. Deiana, C. Schlaup, M. Malizia, T. W. Hansen, S. Horch, I. E. L. Stephens and I. Chorkendorff, Oxygen evolution on well-characterized mass-selected Ru and RuO_2 nanoparticles, *Chem. Sci.*, 2015, **6**(1), 190–196.

28 H. Qi, X. Guan, G. Lei, M. Zhao, H. He, K. Li, G. Zhang, F. Zhang, X. Fan, W. Peng and Y. Li, Bimetallic ZIF-derived Co/N-codoped porous carbon supported ruthenium catalysts for highly efficient hydrogen evolution reaction, *Nanomaterials*, 2021, **11**, 1228.

29 L. Bai, Facile synthesis of porous PtRu colloid for enhanced methanol and ethanol electrooxidation, *J. Sol–Gel Sci. Technol.*, 2022, **103**(1), 118–124.

30 W. Nunthakitgoson, N. Kaewwan, S. Butcha, M. Ketkaew, A. Kuhn and C. Wattanakit, Selective electrochemical detection of cannabidiol (CBD) and tetrahydrocannabinol (THC) at molecular-imprinted mesoporous Pt–Ir surfaces, *Biosens. Bioelectron.*, 2025, **292**, 118103.